



Open Access Articles

High-resolution temperature sensing in the Dead Sea using fiber optics

The Faculty of Oregon State University has made this article openly available.
Please share how this access benefits you. Your story matters.

Citation	Arnon, A., N. G. Lensky, and J. S. Selker (2014), High-resolution temperature sensing in the Dead Sea using fiber optics, Water Resources Research, 50, 1756–1772. doi:10.1002/2013WR014935
DOI	10.1002/2013WR014935
Publisher	American Geophysical Union
Version	Version of Record
Terms of Use	http://cdss.library.oregonstate.edu/sa-termsofuse



Water Resources Research

RESEARCH ARTICLE

10.1002/2013WR014935

Key Points:

- High-resolution temperature profiling in the Dead Sea by means of fiber optics
- Quantitative investigation of the thermal morphology dynamics
- Anticorrelation of metalimnion depth to measured sea level fluctuations

Correspondence to:

N. G. Lensky,
nadavl@gsi.gov.il

Citation:

Arnon, A., N. G. Lensky, and J. S. Selker (2014), High-resolution temperature sensing in the Dead Sea using fiber optics, *Water Resour. Res.*, 50, 1756–1772, doi:10.1002/2013WR014935.

Received 20 OCT 2013

Accepted 5 FEB 2014

Accepted article online 12 FEB 2014

Published online 26 FEB 2014

High-resolution temperature sensing in the Dead Sea using fiber optics

A. Arnon¹, N. G. Lensky¹, and J. S. Selker²

¹Geological Survey of Israel, Jerusalem, Israel, ²Biological & Ecological Engineering, Oregon State University, Corvallis, Oregon, USA

Abstract The thermal stratification of the Dead Sea was observed in high spatial and temporal resolution by means of fiber-optics temperature sensing. The aim of the research was to employ the novel high-resolution profiler in studying the dynamics of the thermal structure of the Dead Sea and the related processes including the investigation of the metalimnion fluctuations. The 18 cm resolution profiling system was placed vertically through the water column supported by a buoy 450 m from shore, from 2 m above to 53 m below the water surface (just above the local seafloor), covering the entire seasonal upper layer (the metalimnion had an average depth of ~20 m). Temperature profiles were recorded every 5 min. The May to July 2012 data set allowed quantitative investigation of the thermal morphology dynamics, including objective definitions of key locations within the metalimnion based on the temperature depth profile and its first and second depth derivatives. Analysis of the fluctuation of the defined metalimnion locations showed strong anticorrelation to measured sea level fluctuations. The slope of the sea level versus metalimnion depth was found to be related to the density ratio of the upper layer and the underlying main water body, according to the prediction of a two-layer model. The heat content of the entire water column was calculated by integrating the temperature profiles. The vertically integrated apparent heat content was seen to vary by 50% in a few hours. These fluctuations were not correlated to the atmospheric heat fluxes, nor to the momentum transfer, but were highly correlated to the metalimnion and the sea level fluctuations ($r = 0.84$). The instantaneous apparent heat flux was 3 orders of magnitude larger than that delivered by radiation, with no direct correlation to the frequency of radiation and wind in the lake. This suggests that the source of the momentary heat flux is lateral advection due to internal waves (with no direct relation to the diurnal cycle). In practice, it is shown that snap-shot profiles of the Dead Sea as obtained with standard thermal profilers will not represent the seasonal typical status in terms of heat content of the upper layer.

1. Introduction

Many lakes show dynamic vertical stratification of their water masses where surface water becomes buoyant due to heating because of a net positive energy balance. Primary energy fluxes are typically gained from solar radiation and heat loss by longwave radiation, as well as transfer of sensible and latent heat with the atmosphere. In contrast, deeper layers of a water body are shielded from the major sources of heat [Boehrer and Schultze, 2008]. Once stratified, the upper layer may become chemically distinct from lower layer. For instance, a surface source might reduce or increase salinity, and in absence of water input salinity generally will increase due to evaporation, which is prominently the case of the current configuration of the Dead Sea. Both temperature and salinity affects the density of the water, while the density gradient between the layers determines the stability of the stratification [Kunze, 2003]. The Dead Sea is a terminal desert lake, located at the lowest terrestrial area on Earth, with its water level at 427 m below mean sea level (in 2013). The lake was meromictic in the past, and became holomictic in the last 30 years, due to the near elimination of inflow from the Jordan River resulting in ~1 m/yr drop in the water level, and increasing salinity. During the winter, the Dead Sea is fully mixed for about 4 months due to cooling to the atmosphere and salinity increase continuously due to evaporation; during the warm season, the Dead Sea is thermally stratified, despite salinity increase due to evaporation [Anati, 1987; Gertman and Hecht, 2002]. In spring and summer, thermal stratification develops and a metalimnion is located at a depth of about 20 m. The maximum temperature and salinity difference between the bottom and upper layer during summer are 12°C and 2.5 kg/m³, respectively [Gertman and Hecht, 2002]. The study of the thermal structure and its dynamics

in a stratified lake, such as the Dead Sea, is needed for understanding the physical processes, including heat and water balances, transport of heat, density, momentum, and internal waves. Quantifying these processes is essential for any plan that involves change of the water or salt balances of the Dead Sea [Gavrieli *et al.*, 2011; Lensky *et al.*, 2010].

1.1. The Transition Layer

Systematic studies of the transition zone's thermal structure of a layered lake demand definitions of location and intensity parameters, which represent significant properties on the morphology of the depth temperature profile. The transition layer between the upper water body (epilimnion) and the lower water body (hypolimnion) in a stratified lake is referred to as the "metalimnion," whereas if a single depth is to be reported to represent the division between layers, the section of highest temperature gradient with depth within the metalimnion is often employed, and may be referred to as the "thermocline" [Bates and Jackson, 1987]. It should be noted that the term thermocline may also be used to represent the whole transition layer, but for the sake of this discussion, we shall employ the definitions presented. While the maximum slope (negative) definition of the thermocline is simple, in practice, smoothing of data (e.g., cubic spline) is typically applied in order to obtain a well-defined derivative [Fiedler, 2010; Kim and Miller, 2007; Palacios *et al.*, 2004]. Beyond the difficulty in computing this value from discrete spatial data, it should be emphasized that the maximum slope is often located just below the upper mixed layer, which is in the upper part of the metalimnion, and thus the location of the thermocline often does not provide representative information of the bulk location or thermal structure of the metalimnion [Wang *et al.*, 2000]. For this reason, the depth of a representative isotherm is commonly used in oceanography as a proxy for determining the depth of the transition layer or the thermocline; the essentially subjective "representative isotherm" is chosen for each region of the ocean [Donguy and Meyers, 1987; Fiedler, 2010; Kessler *et al.*, 1995; Meyers, 1979; Pizarro and Montecinos, 2004; Wang *et al.*, 2000].

Regardless of where the metalimnion or thermocline depth had been identified, any one-parameter description cannot provide insight into intensity or shape of the transition layer. A more complete description requires the definition of parameters, which represent at least the location, intensity, and gross shape of the transition. The first requirement of a systematic description is the location of the transition, necessary, for example, for carrying out a mass balance on the layer. Such a location might be defined in many ways, with common definitions including those presented above (a particular isotherm or the depth of maximum rate of temperature change), or may be more complex including dynamic definitions such as the depth of the isotherm of weighted average temperature. The intensity of the temperature gradient (i.e., °C/m) is highly associated with the rate of thermal transfer across the interface, and thus is critical to the computation of a layer-by-layer heat budget. The magnitude of the thermal gradient, for instance, can illuminate whether the energy exchange between levels is via thermal diffusion, turbulent shear mixing, or unstable double diffuse mixing. Finally, many times the transition is asymmetrical being sharper either immediately below the upper layer, or immediately above the lower layer [Wang *et al.*, 2000]. These asymmetries are also diagnostic of the nature of the mixing processes at the interface, and are useful to quantify it in a reproducible manner.

In this study, we search for a quantitative description of the thermal structure of the transition layer in the Dead Sea, a stratified lake, as representing physical processes related to lake thermal layering. To illustrate the implementation of such metrics, we employ data obtained from a high-resolution temperature sensing observation system, and examine several objective definitions for distinct parameters (locations and intensities) within the metalimnion, and explore the dynamics of these parameters.

1.2. Transition Layers' Depth Fluctuations

The link between the fluctuations of the transition layers' depth and sea level is described in many papers, mostly in ocean studies: anticorrelations are typically found between thermocline depth and sea level (as the sea level rises the thermocline deepens). For example, Bray *et al.* [1997] found that over the Indian, Indonesian, and equatorial Pacific basins, sea level and thermocline seasonal variations were negatively correlated. Chaen and Wyrski [1981] using the 20°C isotherm depth as their definition of the layer division found high (anti) correlation (correlation coefficient of 0.92) to sea level, in the western equatorial Pacific from 1970 to 1975 with monthly resolution.

The anticorrelations of transition layer depth (or the thickness of the upper layer) to sea level is explained using a simplified "two layer system" with known densities and thicknesses, where sea level changes are

synchronized with thermocline depth while approaching hydrostatic conditions by equalizing pressure in the lower water body. *Rebert et al.* [1985] explored the correlations between sea level, thermocline depth, and heat content, along with other parameters, also finding negative correlation between sea level and to thermocline depth. They showed that correlations to thermocline depth were significantly stronger when the thermocline was sharper. The spatial and temporal resolution of these oceanographic studies were coarse (tens of meters in depth and monthly averaged depths and levels). In lakes, the metalimnion depth fluctuations are of frequencies of hours (e.g., the study in Lake Kinneret by *Boegman et al.* [2003]) and the spatial resolution required for exploring these fluctuations must be in a scale that is significantly smaller than the metalimnion thickness (which is typically of only few meters). Accordingly, much greater spatial and temporal resolution of temperature profiling is needed for exploring the metalimnion fluctuations and their correlations to surface level, heat content and water movements in lakes, such as the Dead Sea presented in this study.

1.3. Detailed Temperature Profiling—Using DTS/Fiber Optics

Examining the details and dynamics of temperature profiles in the Dead Sea was done by means of Distributed Temperature Sensing (DTS) using optical fibers. The method of temperature sensing is based on the “Raman”-type scatter of light in optical fibers, where certain properties of the backscattered light are related directly to the temperature at the location of reflection on the fiber. The method is explained in detail by *Selker et al.* [2006].

This technique has been employed in many environmental applications, e.g., stream-aquifer interaction [*Vogt et al.*, 2012], snow energy balance [*Selker et al.*, 2006], soil moisture measurements [*Ciocca et al.*, 2012], borehole monitoring [*Freifeld et al.*, 2008; *Henninges et al.*, 2003] aquifer characterization [*MacFarlane et al.*, 2002], and often provides a solution for cases where high resolution is needed, in time and space simultaneously. The method was also implicated in lake studies; air-water interface profiles of high resolution were investigated in focus of the first two shallow meters [*Selker et al.*, 2006; *Vercauteren et al.*, 2011], and a relatively coarse measurement of a deep (~ 400 m) profile that crossed the stratified lake Tahoe [*Tyler et al.*, 2009], though, neither focused on the stratification of the water body and on the area of the transition layer, between the two main water bodies. *Suárez et al.* [2012] applied a particularly high-resolution DTS for studying the stratification in thermohaline-driven shallow ponds. This was done with an engineered, small-scale system, in different from the current study that focused on a natural, big-scale system as the Dead Sea.

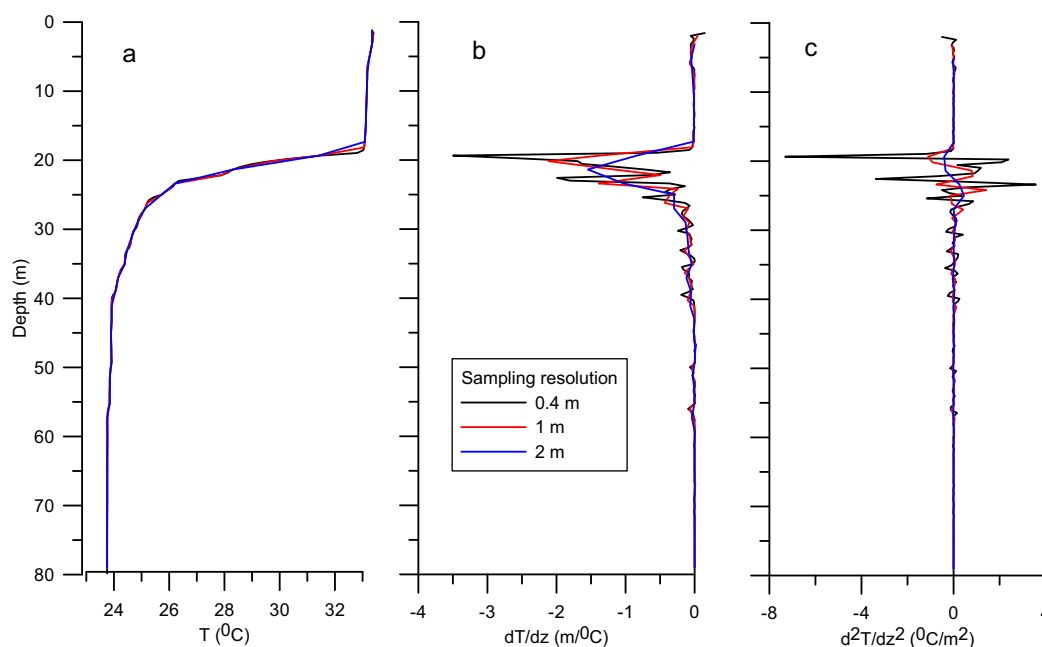


Figure 1. Depth profiles of (a) temperature, and the (b) first and (c) second derivatives, using the original CTD resolution (0.4 m black curves) and degrading resolution (1 m red, 2 m blue), measured in the Dead Sea 21 July 2013 in EG55. Note the degradation of the profile thermal morphological features with the degradation in spatial resolution.

The temperature profile of the Dead Sea has been continuously monitored with a chain of 12 sensors over the upper 40 m for the past two decades [Gertman and Hecht, 2002]. The existing monitoring provides the access to seasonal and long-term variations in the thermal structure of the Dead Sea, which is the basis for heat and water budget calculations [Lensky *et al.*, 2005], and for limnological modeling [Gavrieli *et al.*, 2011]. Yet, the resolution of this monitoring is too coarse for analyzing the dynamics of the irregular thermal stratification, the location of different parts of the metalimnion, and their relation to sea level fluctuations. To demonstrate the requirement of high-resolution temperature profiling for metalimnion research, we present in Figure 1a conductivity-temperature-depth (CTD) temperature profile with computed first depth derivative (sharpness) and second derivative (curvature), using the original spatial resolution (0.4 m) and degradation of resolution of the same profile (1 and 2 m). The figure clearly demonstrates that as the resolution coarsen, more and more features of the thermal morphology are lost (sharpness, curvature, asymmetry, exact location of the thermocline, stairs). It is this critical gap which we seek to fill by applying the fiber optic method to provide finer spatial (submeter) and temporal (minutes) profiling, which covers the upper mixed layer, metalimnion and the lower water body (down to 53 m depth).

1.4. Aims

The aim of this study is to present an experimental methodology of high-resolution thermal profiling, combined with analytical metrics computed from the observations, for understanding the thermal dynamics in a stratified lake. This development is motivated here by the following two specific objectives for the Dead Sea:

1. The exploration of the dynamics of the Dead Sea's thermal structure and the related processes employing a high spatial and temporal resolution temperature sensing method. Using the detailed profiles to define objective parameters of different parts of the metalimnion and examining their dynamics with relation to processes in the lake, e.g., double-diffusive fingered mixing.
2. Investigating, based on the high-resolution approach, the dynamics of the depth fluctuations of the metalimnion and its relation to sea level fluctuations, to heat content and atmospheric boundary conditions.

2. Methods

2.1. System Setup

A high-resolution temperature profiler was designed to continuously record the Dead Sea thermal stratification. The profiler is based on fiber-optics temperature sensing and was designed to cover the entire

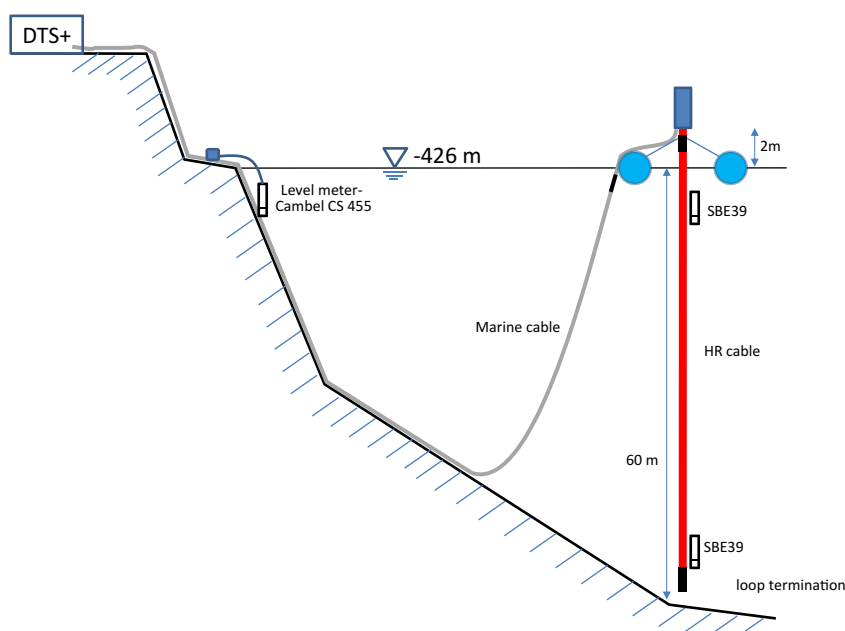


Figure 2. Schematic illustration of the fiber-optic temperature profiling measurement system.

epilimnion and metalimnion and the upper part of the hypolimnion. The lake's metalimnion is located in average at 20–30 m deep [Gertman and Hecht, 2002], so a 53 m profile was employed to capture the three-layer structure.

Two cables and a connection box were specially designed by Brugg Cables (Brugg, Switzerland), to fit the required resolution of this study and to function in the aggressive hot and salty conditions of the Dead Sea. The 55 m profiler is a high-resolution (HR) optic fiber ("BRUsens 70°C high resolution"). The upper 2 m of the profiler were above the water surface, with 53 m submerged. The profiler was 2.5 cm in diameter, helically wrapped high spatial resolution optic fiber cable, hung in the water down from a specially designed anchored buoy, located 450 m offshore near Ein Gedi (Figure 2). The wrapping was about a central 21 mm diameter steel cable with plastic jacketed core. The two wrapped fibers were encased in 2 mm plastic tubes, with one fiber in each tube, which resulted in 1.1 m of each of the two fibers for each 0.1 m of profiler length. The helical wrapping was protected by a 1.5 mm thick urethane jacket. The light was brought to the profiler via a second duplex optical cable, a 600 m long, 10 mm diameter marine cable (Brugg BRUsens Submarine, Brugg, Switzerland). A 316L stainless steel connection box contained E200 barrel which joined the two cables. Both cables were produced using Corning ClearCurve bend-optimized fiber, and terminated with E2000 advanced piston corer (APC) connectors. The polyurethane jacket for both cables was chosen for high mechanical strength and for been smooth, almost entirely preventing halite crystallization, whereas other steel and nylon covered cables quickly become deeply covered by halite. The cables were operated in duplex mode with the light traveling from the shore to the sea to the bottom of the HR cable and (continuously) coming back to the buoy and back to the DTS onshore. The calibration of the vertical cable employed the data from two high-precision data logging pressure and temperature sensors (Seabird 39, accurate to 0.001°C and 0.002 m of water head) attached to the cable 10 and 53 m below the water surface. The pressure data were collected to determine the vertical offsets of the cable due to: (i) vertical offsets of the buoy during wavy times, and (ii) currents that may tilt the cable. The vertical offsets measured were up to 0.15 m, which assures that the offset due to buoy motion is within the range of the vertical spatial (sampling) resolution (± 9 cm) of the optic profiler. A single event of pressure decrease due to current that laterally dragged the cable was observed in the 4th of May 2012 (as will be discussed in the results). This offset can be geometrically corrected in the temperature profile. To conclude, the pressure monitoring assures that the vertical resolution is limited by the profiler resolution (9 cm) and that the buoy and lateral drag of the cable introduce only a minor vertical offset, that if needed can be corrected by pressure data. Changes in gross sea level were simultaneously measured by a pressure sensor (Campbell CS 455 Submersible Pressure Transducer) placed at seafloor in about 3 m of water depth near the shore (Figure 2).

The DTS instrument used in this study was a Sensornet Oryx+ (Sensornet, London, England). The sampling interval was 1 m, and the reported resolution of the device was 2 m. The DTS used in this study was set to record averaging over 5 min balancing minimization noise (found to be 0.02°C in this configuration) while maintaining high enough frequency to observe structural changes in the temperature profile. The absolute accuracy of the DTS temperature measurement depends on the calibration procedure (see below).

The buoy was a catamaran designed to be able to support 1300 kg, ample for carrying the optical cables system and the anchoring cables, including the expected added weight on the anchoring cables due to salt precipitation. The connection box was attached to a vertical pole in the center and top of the construction. Down from the connection box the HR cable was hung vertically and into the water, and the marine 10 mm cable was directed along the buoy construction and into the water toward the shore. The profiler was placed in the center of buoy, which kept vertical offsets smaller than the spatial resolution of the profiler (9 cm). The buoy was secured using four 500 kg concrete anchors attached to the buoy by 8 mm steel cables.

2.2. Calibration

DTS systems must be calibrated to obtain accurate temperature data from the optical signals. Following the procedure described by Hausner *et al.* [2011], calibration requires solving the relation between the ratio of Stokes to Anti-Stokes intensities and the temperature. At position z along the cable, the power of the

measured Raman Stokes, $PS(z)$, and anti-Stokes, $PaS(z)$, signals are translated into temperatures according to:

$$T(z) = \frac{\gamma}{\ln\left(\frac{PS(z)}{PaS(z)}\right) + C - \Delta\alpha z} \quad (1)$$

where γ , C , and $\Delta\alpha$ (the differential attenuation between the anti-Stokes and Stokes signals) are calibration parameters obtained by fitting computed temperatures of equation (1) at locations where the true temperature is known (here via the sensors at 10 and 53 m depth). The magnitude of the signal attenuation is an attribute of the fiber and varies between cables but is usually constant within a single fiber; hence, a specific single-ended calibration was done for the HR vertical cable. Calibration issues related to the special design of the cables are discussed in a technical note (A. Arnon et al., Correction of temperature artifacts in transition to a wrapped optic 1 fiber: Example from Dead Sea, submitted to *Water Resources Research*, 2013). The absolute accuracy of DTS measurements depends on correct calculation of the temperature offset, which accounts for instrument-specific sensor and laser performance. This value is obtained through the data employed in the single-ended attenuation determination, using one of the known temperature points as a reference to calculate an offset of the entire data set.

A spatially constant, time-dependent offset between the SBE39 sensors temperature and the fiber temperatures was observed after employing static calibration parameters. This offset was associated with extreme changes in temperature in the optical connectors within the connection box that was exposed to dramatic heating and cooling during the day and night. The effect was a pure offset, and thus was corrected by adding the difference between the lower SBE sensor measurement and the static calibrated temperature data on the fiber to each of the measurements along the fiber for every reading.

The calibrated profile data sets represent 55 m of cable with 9 cm spacing (of ~ 640 measurement points), which were found to be accurate to $\pm 0.02^\circ\text{C}$, for 5 min integration time. The data from each profile were analyzed to quantitatively investigate the thermal structure dynamics to obtain: (i) the depth of isotherms within the metalimnion; (ii) dT/dz profiles; (iii) $d(dT/dz)/dz$ profiles; and (iv) the integral of temperature (for later computation of profile heat content).

3. Results and Discussion

3.1. The Temperature Profiles: Three Regions

Three major regions with different thermal characteristics appeared in the water column of the Dead Sea during the observation period of May to July 2012 (Figures 3 and 4).

The lower water body was quasi isothermal at a temperature of 23.1°C (as seen in Figures 3–5). This implies that during the presented period the lower water body was effectively thermally isolated from the atmosphere and other heat sources.

The upper water body exchanged heat and mass with the atmosphere and the temperature changed accordingly. Its depth averaged 20 m during the observation period, and warmed up from a maximum temperature of 26°C at the water surface to 36°C over the period of observation (from spring to mid-summer). Daytime shortwave radiation accumulated heat in a relatively shallow layer (< 5 m) which warmed about 3°C each day (Figures 3 and 4). During nighttime, the diurnally warmed layer would mix with the entire roughly 20 m deep upper layer. Occasionally, remnants of the daily warm shallow water did not fully mix, typically leaving less than 1°C in thermal contrast in the upper layer. The temporal mixing pattern fits the typical wind diurnal cycle above the lake, in which the wind is active during nighttime [Nehorai et al., 2009; Gertman and Hecht, 2002]. The diurnal warming of the shallow waters followed by nighttime vertical mixing results in the gradual warming of the whole upper water body.

Finally, the metalimnion transition layer between the relatively uniform upper and lower water bodies consisted of a major thermocline, including a relatively thin layer generally found in its upper portion in which most of the temperature difference occurs including the highest temperature gradient, which we define in this paper as the thermocline. Below the thermocline, the “tail” of the metalimnion appears as a relatively gradual monotonic temperature decrease with depth (Figures 3 and 4). The lower boundary of the metalimnion is gradual to the point of sometimes being indistinct, but given the stable temperature at depth may be defined as the isotherm that is significantly higher than the temperature of the lower water body.

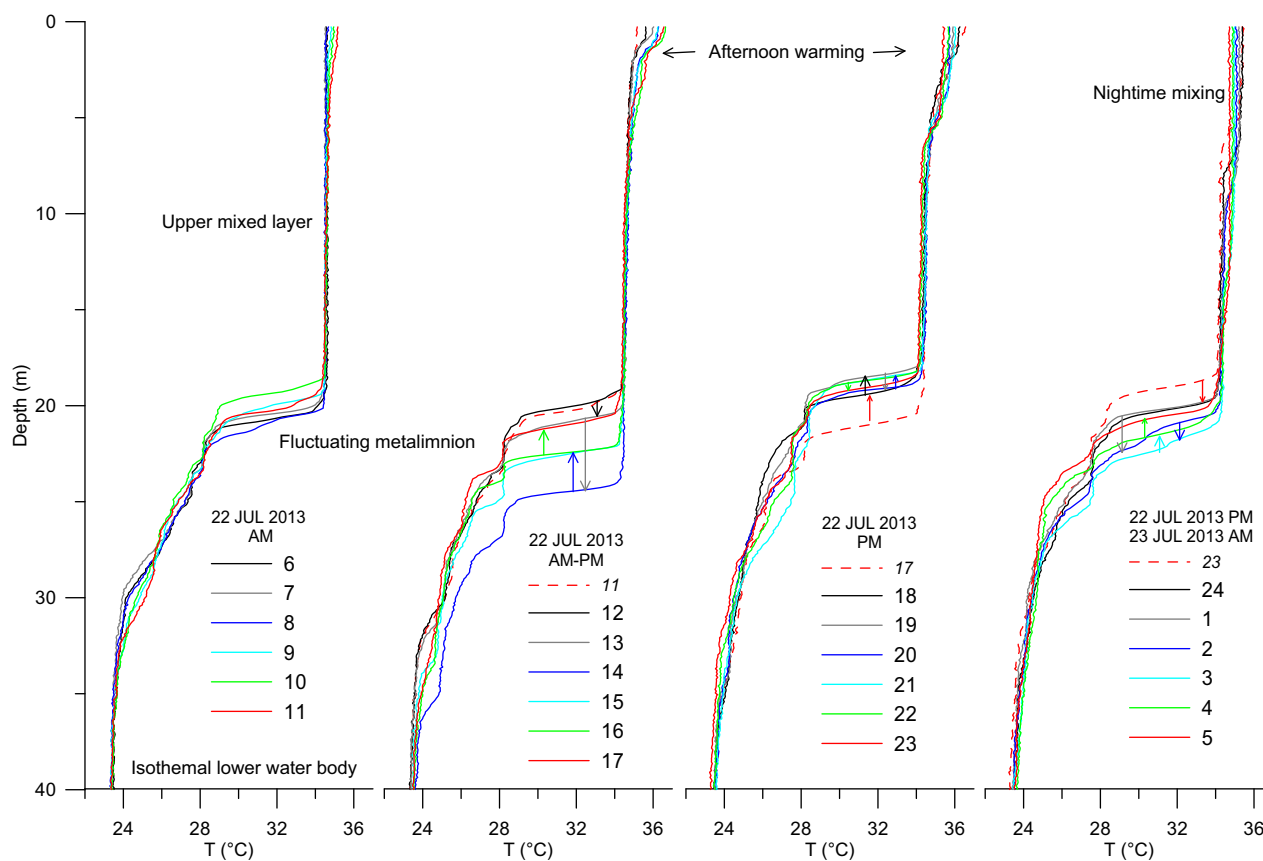


Figure 3. Hourly (GMT+3) temperature depth profiles of the Dead Sea (EG55 station) during 22–23 July 2012. Note the uniform upper layer during late nighttime, and daily warming of the shallow water (<5 m). The metalimnion location changes rapidly (up to 2 m/h).

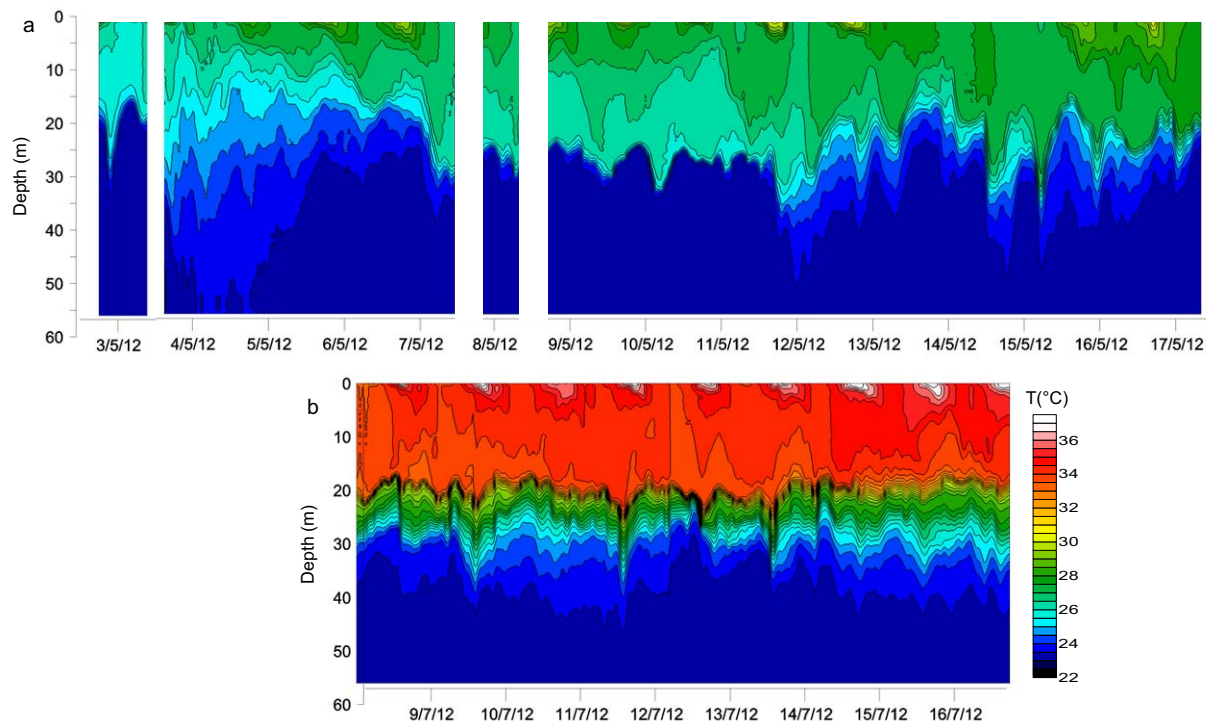


Figure 4. Time series of temperature to depth profiles measured on (a) 3–17 May and (b) 8–16 July. The temperature color scale is on the bottom right. The missing data on the 3rd, 7th, and 8th of May are pauses in data collection due to maintenance of the cables and DTS.

3.2. Metalimnion Morphological Definitions

The thermal structure of the metalimnion is highly dynamic in time, including fluctuation in the depth of the metalimnion and changes of the internal structure within a few hours (Figures 3 and 4). Also, the steepness of the temperature change varies dramatically from a metalimnion that is focused over a few meters in the 3rd of May, to a smeared metalimnion in the 4th of May which spreads over 50 m thickness with no clear thermocline, returning to a sharply changing metalimnion in the following days. Seasonal variations were also observed, for example the May and July temperature profiles are different in the structure and in intensity of change (Figure 4). The morphological changes of the metalimnion profile likely indicate conditions and processes related to lake stratification. Objectively identification of states and transitions in these features is possible here using the high spatial resolution of observation. The first and second derivatives of temperature are well defined and highly informative (Figure 6):

1. The thermocline depth is defined as the location of maximum temperature gradient (dT/dZ) (red arrow).
2. The top of the thermocline is defined as the location of the minimum value of the second depth derivative of temperature, or the maximum convexity of the profile, typically just above the thermocline depth (green arrow).
3. The bottom of the thermocline is similarly defined as the location of the maximum value of the second derivative of temperature, or the maximum concavity of the profile, typically just below the thermocline depth (black arrow).
4. The upper boundary of the metalimnion is defined as the location along the profile where 10% of the temperature difference between the typical upper and lower water bodies is obtained, starting from the top (yellow arrow). This is also considered the base of the upper layer. The temperature of the upper and lower water bodies should be properly defined for each profile. The choice of 10% is somewhat arbitrary, and can be adjusted.
5. The bottom boundary of the metalimnion is similarly defined as the location of which 90% of the temperature difference between the typical upper and lower water bodies is obtained, starting from the top

(purple arrow). This is also defined as the upper boundary of the lower water body.

Another group of parameters that can be investigated over time are parameters related to the shape of the temperature profile. For example, in Figure 7, we show the dynamics of sharpness of the thermocline by presenting the time series of the value of maximum gradient in the profile. The degree of asymmetry of the metalimnion around the major thermocline can be computed as the following ratio: the distance from the maximum gradient to the top boundary of the metalimnion, over the distance from thermocline to the bottom boundary of the metalimnion. If the thermocline is located in the upper part of the metalimnion a value smaller than 1 is obtained, and if it is located in the deeper part of the metalimnion the ratio is bigger than 1. In a symmetric case where the thermocline is centered the value will be close to 1.

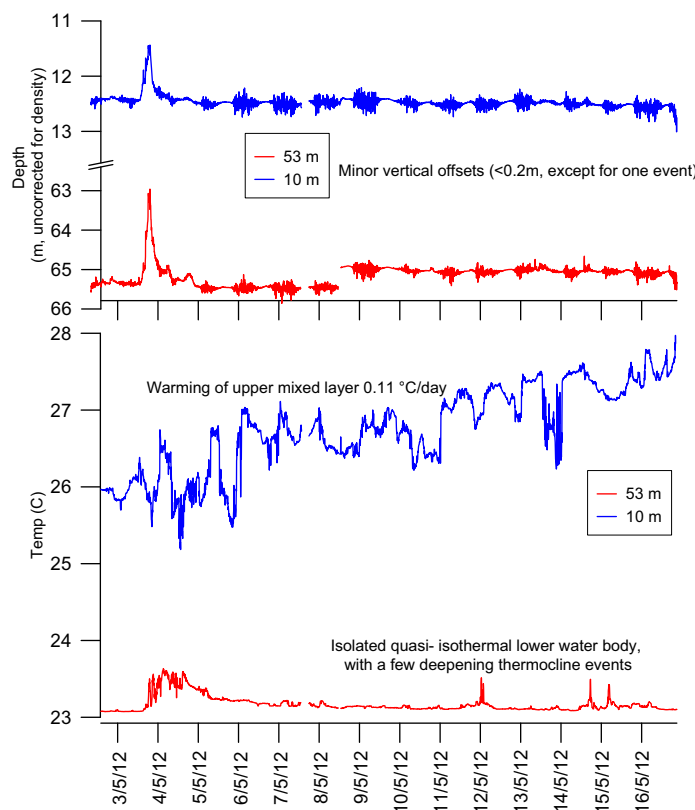


Figure 5. Pressure and temperature data recorded by SBE39 sensors at 10 and 53 m along the fiber-optic profiler.

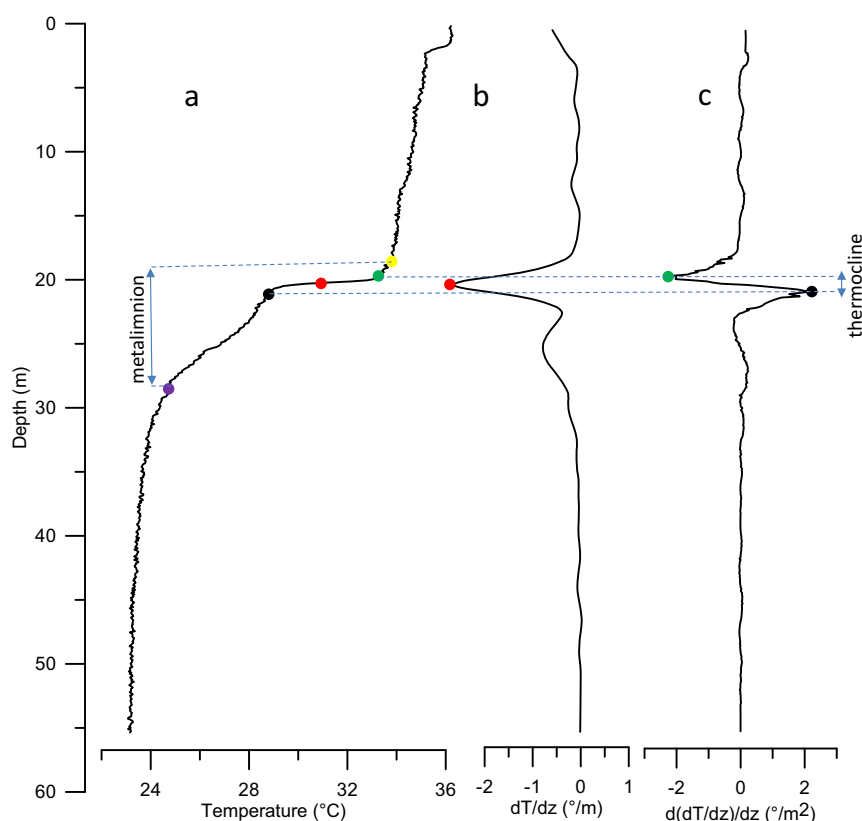


Figure 6. Illustration of the morphology definitions of the metalimnion based on data obtained 20 July 2012 at 14:00. (a) Measured temperature profile, (b) first derivative profile, and (c) second derivative profile. Red dots identify the thermocline, green and black the maximum second derivatives immediately above and below the thermocline, while yellow and purple dots identify the 10% and 90% isotherms relative to the total change in temperature over the metalimnion.

Another approach is to treat the temperature transition like a cumulative probability function, so the derivative of the temperature would be the equivalent of the probability density function for the temperature gradient. Using this approach, one can compute the first (central location), second (standard deviation, or width of the distribution), and third moment (skew, or asymmetry of the distribution). These moments of distribution also address the location and structure of the metalimnion, such as its sharpness (the variance or standard deviation), and asymmetry (skewness). The advantage of this approach is that a classical shape analysis is applied to a high-resolution temperature profile. However, since the calculation of the second and third moments is based on the first central moment, which is equivalent to the location of the temperature weighted average, they do not refer to the location of the maximum gradient in the profile. As for a substitute for the second moment—the width of distribution, we think the intensity of the thermocline itself (value of maximum gradient in the profile) better represents the sharpness of the metalimnion or thermocline, and provides an appropriate metric for examining this feature. Similarly the asymmetry parameter around the thermocline better represents the metalimnion's asymmetry, compared to skewness, which is based on the asymmetry around the first central moment.

More definitions could be considered for each case, such as the location of specific isotherms, and the intensity of the temperature-depth second derivatives. In addition, a special treatment should be taken for “stairs” like thermal structure, in which more than one dominant thermocline exists.

The dynamics of the metalimnion thermal structure, as illustrated using the parametric framework we propose, is presented in Figure 7. The temperature gradient profile time series (Figure 7b) clearly emphasizes the variation in metalimnion location, and also its internal structure; thermocline “stairs” are readily apparent with high (absolute) gradient values whereas uniform areas have low gradient values. It is also clear that the metalimnion thermal structure is typically asymmetrical, with the thermocline at its upper part, and a more moderate temperature decrease below it. This asymmetric structure is expressed in values of degree

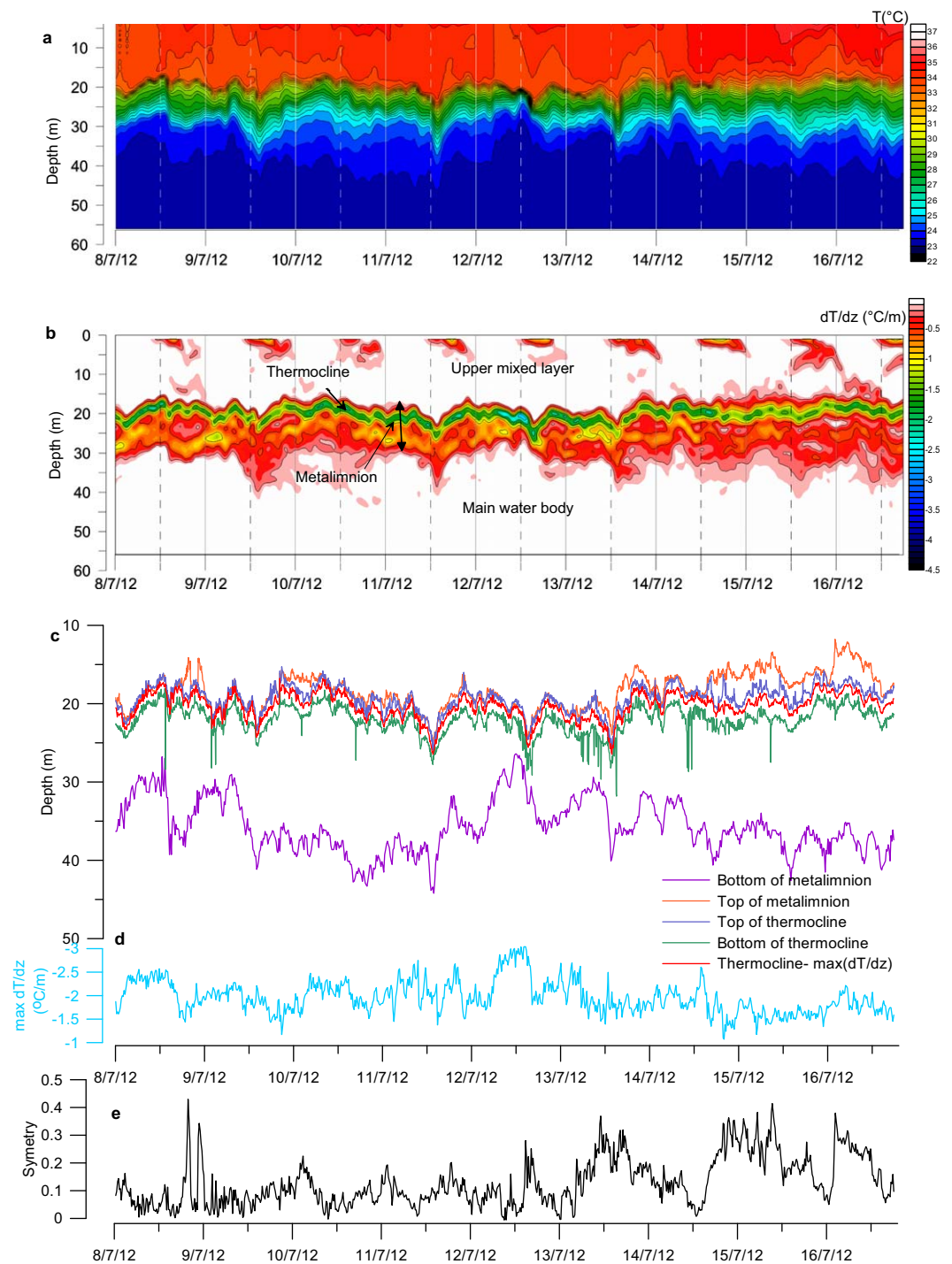


Figure 7. Temperature depth time series observation and its derivatives, 8–16 July 2012: (a) temperature to depth, (b) temperature depth gradient (first derivative), (c) locations of the five chosen parameters for studying the metalimnion structure, (d) the steepness of the thermocline (value of first derivative), and (e) the symmetry metric. Note the solid vertical lines on Figures 7a and 7b mark 12:00 AM and the dashed vertical lines mark 12:00 PM.

of symmetry far less than 1, shown on Figure 7e. The asymmetric is also noticed in Figure 7c, where four out of the five parameters are relatively clustered a couple of meters around the thermocline depth at the upper metalimnion part through the observed period, while the “bottom of the metalimnion” is located relatively far beneath them (~ 15 m). Sharpening (and smearing) of the metalimnion is reflected in shrinkage

(and expanse) of the entire metalimnion thickness (Figure 7b), and in the degree of convergence of the five parameters (Figure 7c). Also, the value of the maximum gradient (minimum for z directed downward) in the profile increases with sharpening, and decreases with smearing, as seen in the bottom of Figure 7c (e.g., in the 12th of July during the afternoon, at which all five parameters are converging, including the 90% temperature difference representing the bottom of the metalimnion. The metalimnion thins and the gradient values rise due to the sharpening).

The diurnal thermocline cycle is also clearly apparent in combining the temperature and temperature gradient time series (Figures 7a and 7b), where high gradients develop around noon time at the top 5 m and deepen afternoon with the increasing of wind intensity (see Figure 9a for wind pattern expressed by the waves amplitude), until it disappears at night. This paper, though, focuses more in the seasonal metalimnion and we will not extend the discussion about the shallow diurnal thermocline.

The dynamics of the metalimnion's structure, as expressed in the time series presented in Figure 7, is likely to be meaningful in understanding processes that are related to the metalimnion depth fluctuations, and the sharpening and smearing of the temperature profiles, such as vertical currents and stair cases due to double-diffusive advection of heat and salt.

The most significant event of deformation of the metalimnion structure in the presented period appeared in the period from the 3rd to the 6th of May 2012, where a metalimnion that was just a few meters thick suddenly "smeared" and expanded to more than 50 m, then a couple of days later was again a relatively thin structure. Simultaneously, a rare single event of tilting of the optical cable by currents was recorded (Figure 8). We thus relate the smearing event to strong currents which resulted in intensive vertical mixing and deformation of the thermocline (and pycnocline). It should be noted that this rare event occurred at the beginning of the layering onset, where the density difference across the pycnocline is still low (as will be presented below). As the upper layer warmed up along the summer, it became less dense, the density gradient increased and the vertical mixing across the pycnocline diminished. The Richardson number (Ri) expresses the ratio of potential to kinetic energy, or the tendency of the lake to remain stratified under shear; when $Ri < 1/4$ velocity shear can overcome the tendency of a stratification, and some mixing (turbulence) will generally occur. Indeed, in the event of May, the conditions favored vertical mixing, with $Ri \sim 0.22$.

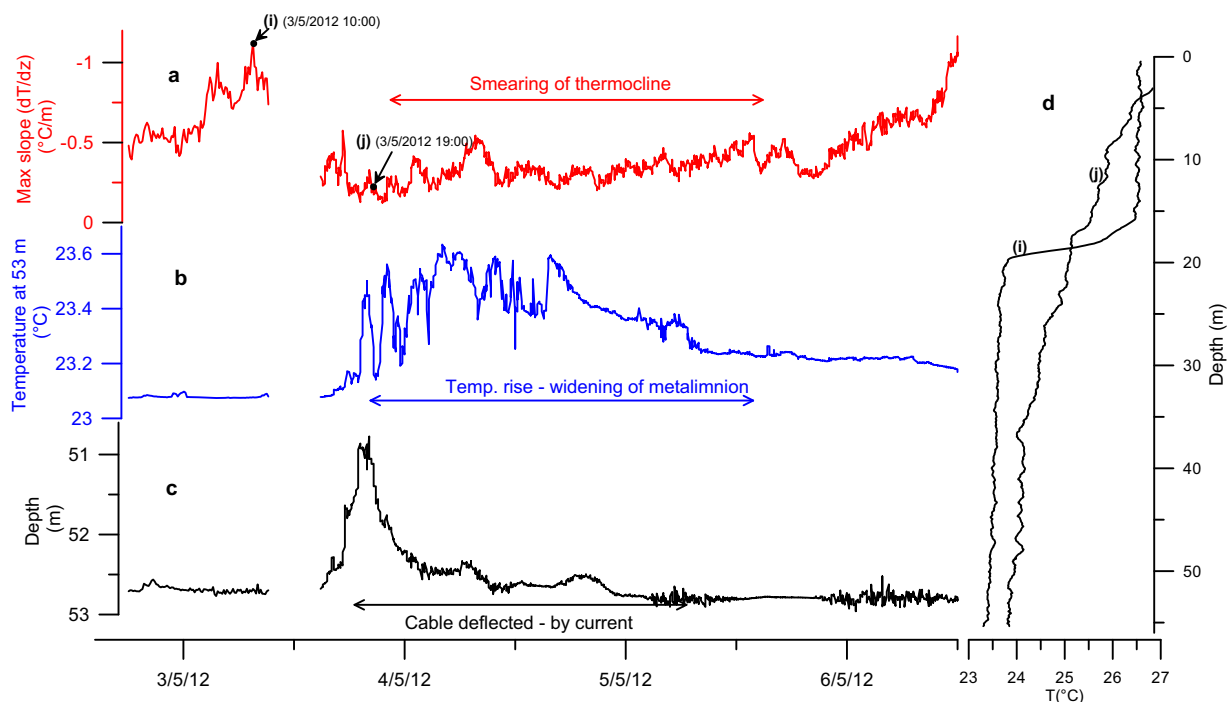


Figure 8. A "smearing event" where simultaneously the thermocline became (a) smoother, while (b) metalimnion bottom was pushed to deeper parts, and (c) the profiler was tilted by current drag the pressure recorded in the lower part of the profiler reduced. (d) Two profiles before and after the "smearing event" as example for the difference in sharpening of the metalimnion. The gap in data on the 3rd of May noontime is due to cable maintenance.

(density difference ~ 0.5 sigma, current intensity considered ~ 0.3 m/s), while later in mid-summer (July), the stability of layering was dominant, with $Ri > 0.67$ (density difference ~ 1.5 sigma, and same current value).

3.3. Thermocline Depth Fluctuations

3.3.1. Anticorrelation of Thermocline Depth to Sea Level Fluctuations

In addition to the changes in the structure of the metalimnion, the location of the entire metalimnion (as expressed in the location of the defined parameters) fluctuates significantly throughout the measured periods within hours (Figures 3 and 7). The amplitude of the metalimnion fluctuations is up to 15 m during May and up to 7 m during July. These fluctuations change the average 20 m thickness of the upper warm water layer by up to 28% and 60%, respectively. Thus the calculated heat content of a measured profile changes dramatically during these fluctuations, and the resulted heat content will depend on the metalimnion depth at the observation time. We found systematic anticorrelation between metalimnion depth fluctuations and the sea level fluctuations. We define this as anticorrelation since the movements of the two interfaces are in opposite directions, when the water level rise the thermocline deepens and vice versa. The sea level time series was detrended in order to filter out level decline due to the negative water balance of the lake, before performing the correlations. In addition, we filtered out the short period (seconds) wave action signal. The results of the anticorrelations of sea level to metalimnion depth in the five parameters discussed above are presented in Table 1. The highest anticorrelation of sea level was obtained with the thermocline depth (maximum dT/dZ). In addition, we checked the anticorrelation of the depth fluctuations of isotherms within the metalimnion (from 24°C to 32°C in steps of 0.25°C) to the level changes. Interestingly, isotherm 28°C , which is located below the “thermocline depth” during the presented period, reveals the highest anticorrelation with level changes ($r = 0.84$), even higher than the thermocline depth ($r = 0.74$).

Figure 9 presents the time series of the metalimnion depth (represented by isotherm 28°C), and level fluctuations throughout the period of 8–17 July. The high anticorrelation of the two series (0.84) is clear, and is expressed in the major as well as in the minor trends of the series. The diurnal atmospheric forcing of radiation and wave intensity throughout the observed period are presented on the upper part of the figure. These atmospheric forcing time series are not correlated to sea level fluctuations nor to metalimnion depth (level and metalimnion depth, $R < 0.2$).

The movement of the metalimnion, as the boundary between the two layers, changes the ratio between the mass of cold-dense water and the warm-less dense water in the measured water column. As mentioned in the introduction, the location of this boundary is shown to be anticorrelated to the sea level, related to maintaining hydrostatic conditions when the mass (and therefore the pressure) of the water column changes due to addition/reduction of water following wind patterns that form level changes. In an ideal two-layer system with an upper layer of depth D , density ρ_1 , and a lower layer of density $\rho_2 = \rho_1 + \Delta\rho$, and hydrostatic conditions are fulfilled, changes in sea level Δh and changes in the upper-layer depth ΔD are related by $\Delta h = \Delta D \cdot \frac{\Delta\rho}{\rho_1}$ [Wyrki and Kendall, 1967]. In the case of the Dead Sea, we found that as the upper layer becomes less dense along the warm season (from spring toward mid-summer), the amplitudes of the upper-layer depth decrease (from ~ 15 m in May to ~ 7 m during July), while the lake level fluctuations remains in the same range (± 1 cm).

Figure 10 presents the measured level fluctuations versus the depth of the metalimnion (represented by isotherm 28°C), showing a linear trend, where the slope of the linear regression is the measured $\Delta h/\Delta D$ ratio typical for the examined period. This ratio is equal to the density ratio $\Delta\rho/\rho_1$, if hydrostatic conditions are achieved. The density of the upper and lower water masses were measured along the season, using a density meter Anton-Paar DMA5000 (following the procedure of Gertman and Hecht [2002]). Table 2

Table 1. Anticorrelation of Metalimnion Depth to Sea Level

Boundary Depth Criterion	Anticorrelation to Level
Max dT/dZ	0.74
Max second derivative (top of thermocline)	0.72
Min second derivative (bottom of thermocline)	0.58
Top of metalimnion—90% difference	0.58
Bottom of metalimnion—90% difference	0.43
Isotherm 28°C	0.84
Heat content	0.84

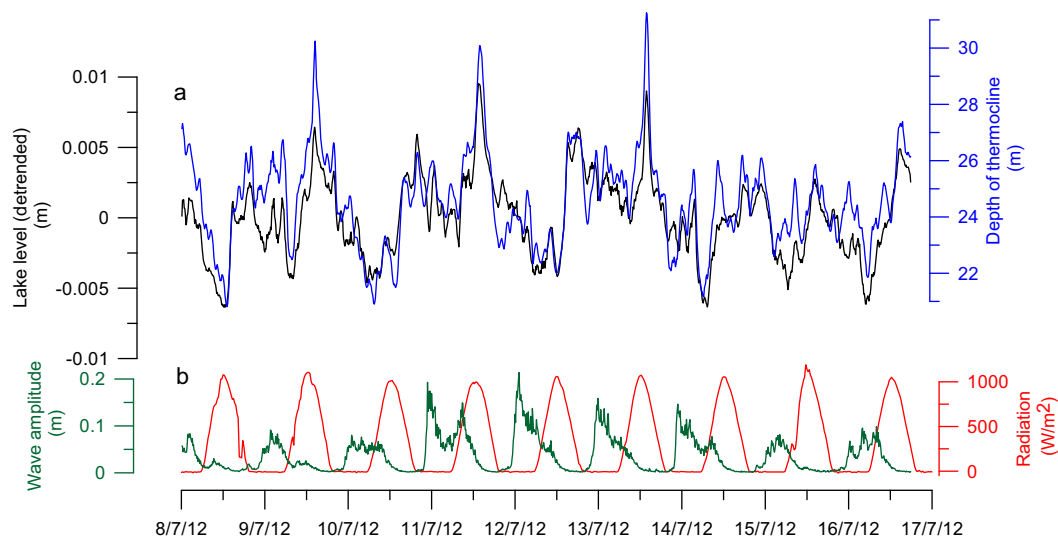


Figure 9. (a) Sea level and metalimnion depth (represented by isotherm 28°C) time series are highly anticorrelated ($r = 0.84$) during 8–17 July together with (b) measured radiation and wave amplitude which are not correlated to both sea level and metalimnion depth.

includes the ratio $\Delta h/\Delta D$, calculated for three periods in May, June, and July 2012 from the fiber data and sea level measurements throughout each period. In addition, Table 2 gathers data of typical temperature, salinity, and density of the two water bodies with the ratio $\Delta\rho/\rho_1$ measured on three sampling days, each within the fitting period of continues profiling. We found that the measured ratios $\Delta h/\Delta D$ and $\Delta\rho/\rho_1$ are very similar for each period. Thus the two-layer system hydrostatic model explains the majority of the fluctuations of the metalimnion in the Dead Sea with level changes, through the seasonal thermohaline development of the layers.

This section described three important phenomenon in the lake: (a) Dramatic fluctuations of the upper-layer depth (as expressed in the dynamics of all five location parameters and the isotherms), (b) very high correlation of those fluctuations to level fluctuations, and (c) a seasonal adjustment to the stability increase

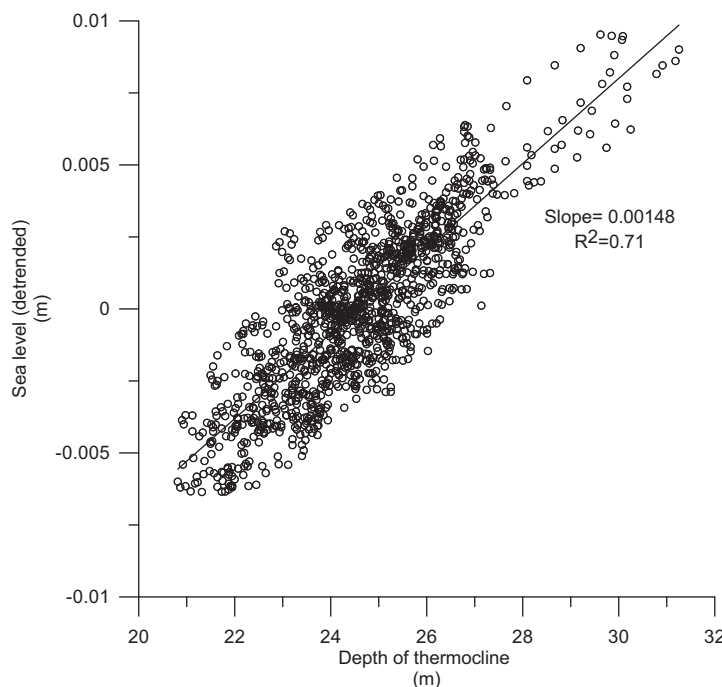


Figure 10. Sea level versus depth of the metalimnion (represented by isotherm 28°C). (From the data shown in Figure 9.)

Table 2. Correlation Slope and Densities for Three Following Periods^a

	$\Delta h/\Delta D$	$\frac{\rho_2 - \rho_1}{\rho_1}$	T_{UL} (°C)	T_{BL} (°C)	S_{UL} (σ ₃₂)	S_{BL} (σ ₃₂)	ρ_{UL} (kg/m ³)	ρ_{BL} (kg/m ³)	R (correlation strength)
May	0.0006	0.00066	26.7	23.1	1238.58	1237.90	1240.86	1241.68	0.70
June	0.0013	0.00144	31.6	23.1	1239.73	1237.89	1239.92	1241.72	0.74
July	0.0015	0.00145	34.5	23.2	1241.22	1238.13	1240.13	1241.93	0.84

^a T_{UL} , S_{UL} , and ρ_{UL} stand for the temperature, salinity, and density of the upper layer. T_{BL} , S_{BL} , and ρ_{BL} —the same for the bottom layer.

of the lake. These three phenomenon require the existence of significant lateral flow of water occurring in relation to maintenance of hydrostatic pressure compensation. In the next section, we will discuss the lateral flow and lateral heat advection.

3.3.2. The Heat Content in the Water Column and Net Heat Flux

In introducing this new approach to profiling lake temperatures, we would like to also demonstrate the transformative opportunities that these data afford. We will introduce a metric of total profile heat content (TPHC), which reveals the fundamental importance of including effects of internal waves in the Dead Sea system. The TPHC of the water column was calculated by integrating the departure of the entire temperature profile from a 0°C profile. In these calculations, the heat capacity of the Dead Sea fluid was taken as 3,030,000 J/(°C·m³), [Steinhorn and Gat, 1983]. The calculations were “area-specific heat” made on a per square meter basis. The small changes of density across the thermocline (~1/1240) are negligible in the context of the TPHC calculations, and thus density was taken as constant along the profile. From this, we could compute the net heat flux into or out of the profile as the time derivative of the heat content (based on 5 min intervals) (Figure 11). In stratified aquatic systems, the major heat flux is typically from the atmosphere through the water-air interface. Nevertheless there is no correlation (<0.2) of the TPHC time series to the net radiation heat flux, nor to the wave’s amplitude, which mix the heat into the upper layer. The heat content time series is highly correlated to the thermocline depth time series (Figure 11), with fluctuations of 50% and more in the TPHC and thermocline depth in periods of a few hours. The two time series were found to be 84% correlated (during the same period of July 2012). This integrative approach revealed better correlations to sea level fluctuations than the parameters of the differential approach including the depth of maximum temperature depth gradient. The improvement of the correlation can be understood by

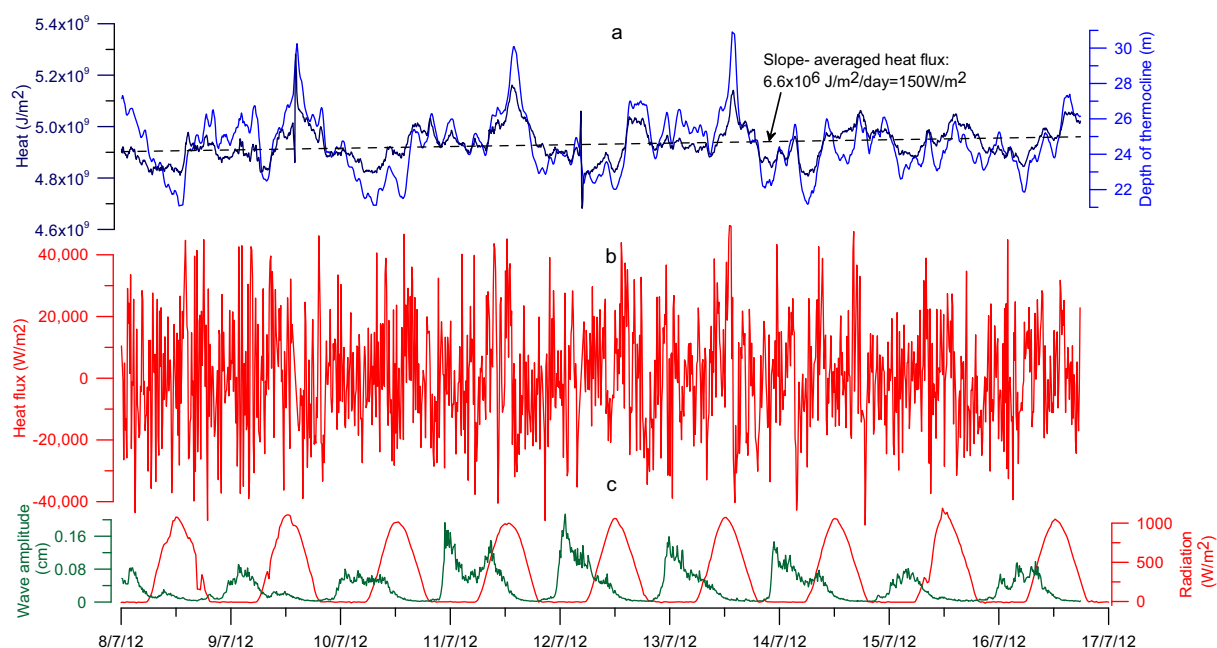


Figure 11. Measured heat and heat fluxes: (a) the dynamics of heat storage in the Dead Sea water column (upper 53 m) and depth of the thermocline (note the high correlation), the dashed line is the linear trend of the heat and its slope represents the averaged heat flux, (b) the net heat flux (calculated as the time derivative of the heat storage), and (c) the incoming solar radiation and wave amplitude, shown as indicators of radiative flux and energy for mixing.

recognizing that TPHC calculation takes into account the entire variations of heat, and therefore density, in the upper layer, including daily changes of the very shallow waters. These daily variations in heat and density are not necessarily expressed in the fluctuations of the main thermocline or any other isotherm.

The net heat flux was calculated from the heat storage time derivative in two ways: (i) the momentary net heat flux time series (5 min represented by a pair of successive measurements); and (ii) running 10 days averaged net heat flux, both presented in Figure 11. The momentary net heat flux is very noisy with momentary heat fluxes in the range of $\pm 40,000 \text{ W/m}^2$, and amplitude up to 40 times higher than the maximum incoming solar radiation. The flux polarity is not correlated to the diurnal radiative net heat flux. However, there is a general trend of increasing stored heat, reflecting the net heat flux gained from the atmosphere through the lake surface. The slope of the general linear trend is of $6.6 \times 10^6 \text{ J/m}^2\text{d}$, which is 150 W/m^2 , distributed along the upper $\sim 20 \text{ m}$ water column (since the gradual rise in temperature characterizes the upper water layer only). The same value of average net heat flux is achieved from the average daily temperature increase of $\sim 0.1^\circ\text{C/d}$ as measured in the 10 m deep thermometer (placed on the fiber), multiplied by the average thermocline depth (and heat capacity and density).

The momentary heat flux is more than 2 orders of magnitude larger than the daily averaged heat flux. Also, the heat storage in the upper 53 m correlates well with the thermoclines fluctuations. Thus we suggest that the rapid shifts in the heat content did not represent the gain or loss of heat from the atmosphere, but rather lateral heat advection within the upper layer. The vertical offsets of the thermocline are compensated by lateral advection, following heat and mass conservation. It should be noted that the heat advection from water inflows (tributaries etc.) into the Dead Sea are negligible [Lensky *et al.*, 2005].

In conclusion, we hypothesize that the correlation of thermocline depth with the heat content of the entire water column and the sea level fluctuations is a dynamic phenomenon of internal waves which explains the measured net heat flux. The thermocline fluctuations represent a complicated 3-D motion of the thermocline surface, which keeps a relationship to sea level to approximate hydrostatic conditions. Applying a 1-D heat balance calculations without considering these factors based on a single profile could result in significant errors (60% in the heat storage) with respect to the representative temporally averaged value.

4. Summary and Conclusions

The morphology of thermal stratification in water bodies is complex, reflecting the many processes contributing to their formation and destruction. In the case of saline systems such as the Dead Sea during summer, for instance, an upper layer may become both more buoyant and higher in salinity, giving rise to double-diffuse instability at the lower interface. This behavior greatly influences the energy balance of the upper layer, and thus heat balance and rates of evaporation and changes in salinity. To understand these complex processes requires that they be observed across the scales at which they are manifest, typically 0.1 m to 10's of meters. The goal of this work was to present a methodology for such observations based on temperature, and explore how to employ these data to draw meaningful conclusions. High-resolution (18 cm at 640 nodes; 5 min over 3 months; 0.02°C) temperature profiles were achieved using DTS under the harsh conditions of the Dead Sea.

Depth profiles of temperature and temperature gradients are presented, including their time series, from which the thermal structure and its dynamics is expressed graphically and serve as a first-order strategy for identification of formative processes. We examined objective parameters for quantifying the thermal morphology of the metalimnion, such as the width of the transition zone, its sharpness, curvature, the degree of asymmetry. Using these parameters, the dynamics of the thermal morphology can be computed based on the high-resolution data. The parameters examined here include the following:

Metalimnion: (i) the depth of top and bottom boundaries of the transition zone, where chosen here are the 10% and 90% isotherms relative to the total change in temperature over the metalimnion; (ii) asymmetry/skewness of the metalimnion (the ratio of distance from the thermocline to the top and bottom boundaries of the metalimnion).

Thermocline: (i) depth of center of thermocline is located at max dT/dz ; (ii) sharpness maximum is the value of max dT/dz ; (iii) depth of top and bottom thermocline boundaries are located at d^2T/dz^2 max and min.

These parameters are presented as time series, which are used to follow the dynamics of the thermal morphology along time, and can be used to examine hypotheses on the dynamics of thermohaline stratification (e.g., the relation of the thermal structure to saline-thermal mass and energy transfer processes seen in hypersaline water bodies).

We found that in the Dead Sea, over the onset of summer conditions, the metalimnion shape and depth changes dramatically. Metalimnion depth fluctuated by ~ 10 m within periods of a few hours, negatively correlated ($r = -0.84$) to sea level, which fluctuated by ~ 1 cm. We examined these fluctuations in the framework of a two-layer hydrostatic model which well predicted the magnitude of the negative correlation of the thermocline depth to sea level. We also found that the thermocline depth is not correlated to the diurnal heat fluxes across the upper boundary of the lake ($r = 0.2$). The amplitude of the thermocline fluctuations was strongly seasonal, from 15 m in May to 7 m in July. These amplitudes are related to the density ratio of the upper and lower layers with correlation coefficients of >0.74 .

The heat content of the water column was calculated for each 5 min profile by integrating the total thermal energy in the water column, and were highly correlated to thermocline depth and to sea level, but not correlated to the diurnal atmospheric heat fluxes. The net apparent heat flux of the vertical thermal profile (the time derivative of heat content) fluctuates by $\pm 40,000$ W/m² within hours. These fluctuations are not correlated in time to the atmospheric heat fluxes, and are about 3–4 orders of magnitude higher than the flux exchange across the air-water boundary. As pointed out above, these fluxes were highly correlated to sea level fluctuations ($r = 0.84$) and thermocline depth. Therefore we suggest that measured net heat flux (temperature integral), which represents the thickness changes of the upper layer, derives from lateral advection source rather than from heat fluxes from atmosphere. The diurnal cycle, which is influenced by atmospheric fluxes, is recognized only in the upper 5–10 m, separated from the location of the dominant thermocline. Because the advected energy fluxes were commonly 3–4 orders of magnitude greater than energy fluxes across the sea surface, the influence of the external energetic forcings (i.e., net radiation and latent heat) on the entire upper layer could be identified and estimated only when looking at periods of many days.

Here we have focused on distinguishing between processes using purely analytical strategies (e.g., an energy balance). We see the potential of these high-resolution data to be even greater in combination with numerical simulations of the complex mixing occurring at the thermodynamically unstable high-shear interfaces found in many saline systems. The instrumentation used here was entirely adequate for this investigation, but by no means represents the limits of this technology. DTS systems with 8 times greater spatial resolution and more than 10 times greater temporal resolution are now on the market which raise the possibility of observation of turbulent mixing on the 1 s time scale, opening the possibility of even greater power to distinguish between subtle processes in such fascinating and important hydrodynamic systems.

Acknowledgments

We thank the Taglit R/V team: Silvi Gonen, Meir Yifrach, and Shachar Gan-El for their construction of the buoy and its maintenance, Isaac Gertman and Tal Ozer for their assistance and guidance of the buoy construction, Raanan Bodzin and Hallel Lutsky for their field and technical assistance, Ittai Gavrieli, Vladimir Lyakhovsky, and Yona Dvorkin for fruitful discussions, Camille Lousqui, Ariel Balmas, Ira Peer, and Yoram Biton for the support in administrative assistance, and Thomas Hertig for discussions on the proper design of the optical cables. We also thank all of the students that joined us and helped with the tough field work in the Dead Sea. We also thank Eyal Shalev and two more anonymous reviewers for their useful comments that significantly improved the manuscript.

References

- Anati, D. A. (1987), Salinity profiles in steady-state solar ponds, *Solar Energy*, 38(3), 159–163.
- Bates, R. L., and J. A. Jackson (1987), *Glossary of Geology*, 3rd ed., Am. Geol. Inst., Alexandria, Va.
- Boegman, L., J. Imberger, G. N. Ivey, and J. P. Antenucci (2003), High-frequency internal waves in large stratified lakes, *Limnol. Oceanogr. Methods*, 48(2), 895–919.
- Boehrer, B., and M. Schultze (2008), Stratification of lakes, *Rev. Geophys.*, 46, RG2005, doi:10.1029/2006RG000210.
- Bray, N. A., S. E. Wijffels, J. C. Chong, M. Fieux, S. Hautala, G. Meyers, and W. M. L. Morawitz (1997), Characteristics of the Indo-Pacific throughflow in the eastern Indian Ocean, *Geophys. Res. Lett.*, 24(21), 2569–2572.
- Chaen, M., and K. Wyrski (1981), The 20°C isotherm depth and sea level in the western equatorial pacific, *J. Oceanogr. Soc. Jpn.*, 37(4), 198–200.
- Ciocca, F., I. Lunati, N. Van de Giesen, and M. B. Parlange (2012), Heated optical fiber for distributed soil-moisture measurements: A lysimeter experiment, *Vadose Zone J.*, 11(4), 1–10.
- Donguy, J. R., and G. Meyers (1987), Observed and modelled topography of the 20°C isotherm in the tropical pacific, *Oceanol. Acta*, 10, 41–48.
- Fiedler, P. C. (2010), Comparison of objective descriptions of the thermocline, *Limnol. Oceanogr. Methods*, 8, 313–325.
- Freifeld, B. M., S. Finsterle, T. C. Onstott, P. Toole, and L. M. Pratt (2008), Ground surface temperature reconstructions: Using in situ estimates for thermal conductivity acquired with a fiber-optic distributed thermal perturbation sensor, *Geophys. Res. Lett.*, 35, L14309, doi: 10.1029/2008GL034762.
- Gavrieli, I., et al. (2011), Red Sea to Dead Sea water conveyance (RSDSC) study: Dead Sea Research Team, *Rep. GSI/10/2011*, Tahal Group and Geol. Surv. of Isr., Jerusalem, Israel.
- Gertman, I., and A. Hecht (2002), The Dead Sea hydrography from 1992 to 2000, *J. Mar. Syst.*, 35(3–4), 169–181.
- Hausner, M. B., F. Suárez, K. E. Glander, N. van de Giesen, J. S. Selker, and S. W. Tyler (2011), Calibrating single-ended fiber-optic Raman spectra distributed temperature sensing data, *Sensors*, 11, 10859–10879.
- Henningses, J., S. Böde, J. Schrötter, K. Erbas, E. Huenges, and M. W. Group (2003), Permanent installation of fibre-optic DTS-cables in boreholes for temperature monitoring, paper presented at EGS-AGU-EUG Joint Assembly, EGS, Nice, France.

- Kessler, W. S., M. J. McPhaden, and K. M. Weickmann (1995), Forcing of intraseasonal Kelvin waves in the equatorial Pacific, *J. Geophys. Res.*, **100**(C6), 10,613–10,631.
- Kim, H.-J., and A. J. Miller (2007), Did the thermocline deepen in the California Current after the 1976/77 climate regime shift?, *J. Phys. Oceanogr.*, **37**(6), 1733–1739.
- Kunze, E. (2003), A review of oceanic salt-fingering theory, *Prog. Oceanogr.*, **56**(3–4), 399–417.
- Lensky, N. G., Y. Dvorkin, V. Lyakhovsky, I. Gertman, and I. Gavrieli (2005), Water, salt, and energy balances of the Dead Sea, *Water Resour. Res.*, **41**, W12418, doi:10.1029/2005WR004084.
- Lensky, N. G., I. Gertman, Z. Rosentraub, I. M. Lensky, I. Gavrieli, R. Calvo, and O. Katz (2010), Alternative dumping sites in the Dead Sea for harvested salt from pond 5, *Rep. GSI/05/2010*, Geol. Surv. of Isr., Jerusalem, Israel.
- MacFarlane, A. P., A. Förster, D. F. Merriam, J. Schrötter, and J. M. Healey (2002), Monitoring artificially stimulated fluid movement in the Cretaceous Dakota aquifer, western Kansas, *Hydrogeol. J.*, **10**(6), 662–673.
- Meyers, G. (1979), Annual variation in the slope of the 14°C isotherm along the equator in the Pacific Ocean, *J. Phys. Oceanogr.*, **9**(5), 885–891.
- Nehorai, R., I. M. Lensky, N. G. Lensky, and S. Shiff (2009), Remote sensing of the Dead Sea surface temperature, *J. Geophys. Res.*, **114**, C05021, doi:10.1029/2008JC005196.
- Palacios, D. M., S. J. Bograd, R. Mendelssohn, and F. B. Schwing (2004), Long-term and seasonal trends in stratification in the California Current, 1950–1993, *J. Geophys. Res.*, **109**, C10016, doi:10.1029/2004JC002380.
- Pizarro, O., and A. Montecinos (2004), Interdecadal variability of the thermocline along the west coast of South America, *Geophys. Res. Lett.*, **31**, L20307, doi:10.1029/2004GL020998.
- Rebert, J. P., J. R. Donguy, G. Eldin, and K. Wyrtki (1985), Relations between sea level, thermocline depth, heat content, and dynamic height in the tropical Pacific Ocean, *J. Geophys. Res.*, **90**(C6), 11,719–11,725.
- Selker, J. S., L. Thévenaz, H. Huwald, A. Mallet, W. Luxemburg, N. van de Giesen, M. Stejskal, J. Zeman, M. Westhoff, and M. B. Parlange (2006), Distributed fiber-optic temperature sensing for hydrologic systems, *Water Resour. Res.*, **42**, W12202, doi:10.1029/2006WR005326.
- Steinhorn, I., and J. R. Gat (1983), The Dead Sea, *Sci. Am.*, **249**(4), 102–109.
- Suárez, F., J. E. Aravena, M. B. Hausner, A. E. Childress, and S. W. Tyler (2012), Assessment of a vertical high-resolution distributed-temperature sensing system in a shallow thermohaline environment, *Hydrol. Earth Syst. Sci.*, **15**, 1081–1093.
- Tyler, S. W., J. S. Selker, M. B. Hausner, C. E. Hatch, T. Torgersen, C. E. Thodal, and S. G. Schladow (2009), Environmental temperature sensing using Raman spectra DTS fiber-optic methods, *Water Resour. Res.*, **45**, W00D23, doi:10.1029/2008WR007052.
- Vercauteren, N., H. Huwald, E. Bou-Zeid, J. S. Selker, U. Lemmin, M. B. Parlange, and I. Lunati (2011), Evolution of superficial lake water temperature profile under diurnal radiative forcing, *Water Resour. Res.*, **47**, W09522, doi:10.1029/2011WR010529.
- Vogt, T., M. Schirmer, and O. A. Cirpka (2012), Investigating riparian groundwater flow close to a losing river using diurnal temperature oscillations at high vertical resolution, *Hydrol. Earth Syst. Sci.*, **16**, 473–487.
- Wang, B., R. Wu, and R. Lukas (2000), Annual adjustment of the Thermocline in the Tropical Pacific Ocean, *J. Clim.*, **13**(3), 596–616.
- Wyrtki, K., and R. Kendall (1967), Transports of the Pacific Equatorial Countercurrent, *J. Geophys. Res.*, **72**(8), 2073–2076.